Electronic Supplementary Material to: Evaluation of Arctic Sea-ice Cover and Thickness Simulated by MITgcm*

Fei ZHENG[1,2], Yue SUN[1,3], Qinghua YANG[4], and Longjiang MU[5]

[1]*International Center for Climate and Environment Science*, *Institute of Atmospheric Physics*, *Chinese Academy of Sciences*, *Beijing* 100029, *China*

[2]*Collaborative Innovation Center on Forecast and Evaluation of Meteorological Disasters*, *Nanjing University of Information Science and Technology*, *Nanjing* 210044, *China*

[3]*University of Chinese Academy of Sciences*, *Beijing* 100049, *China*

[4]*Guangdong Province Key Laboratory for Climate Change and Natural Disaster Studies*, *and School of Atmospheric Sciences*, *Sun Yat-sen University*, *Zhuhai* 519082, *China*

[5]*Alfred Wegener Institute*, *Helmholtz Centre for Polar and Marine Research*, *Bremerhaven* 27515, *Germany*

ESM to: Zheng, F., Y. Sun, Q. H. Yang, and L. J. Mu, 2021: Evaluation of Arctic sea-ice cover and thickness simulated by MITgcm. *Adv. Atmos. Sci.*, **38**(1), 29–48, https://doi.org/10.1007/s00376-020-9223-6.

1. Introduction

This file provides supplementary material on (1) the configuration of MITgcm, and (2) evaluation results by comparing model outputs against three observation datasets individually.

2. MITgcm

The dynamic and thermodynamic sea-ice model based on Zhang and Hibler (1997) is coupled to the ocean component of MITgcm (Marshall et al., 1997a, b). The heat, freshwater fluxes and surface wind stresses are computed from the atmosphere and modified by the ice model every six hours. The internal stresses of the sea ice are calculated following a viscous-plastic rheology (Hibler, 1979). A "zero-layer" model is introduced for the thermodynamic framework, with a linear temperature profile and zero heat capacity for ice (Semtner, 1975). Seven thickness categories are adopted to parameterize a sub-grid scale sea-ice thickness distribution for heat flux computations (Losch et al., 2010). The model is integrated on the Arakawa C grid using a finite volume discretization. A cube-sphere grid projection is employed, which helps to prevent polar singularities (Adcroft et al., 2004). The horizontal model domain is one face of the cube sphere and comprises locally orthogonal 420 by 384 grid cells with a mean horizontal grid spacing of 18 km, with open boundaries in the Pacific and Atlantic oceans at approximately 55°N. There are 50 vertical levels with an approximately 10 m resolution in the upper levels and 400 m resolution in the bottom levels. The bathymetry data are from the U.S. National Geophysical Data (NGDC) 2 arcminute global relief dataset (ETOPO2) (Smith and Sandwell, 1997). The values of the open water, dry ice, wet ice, dry snow, and wet snow albedos are 0.16, 0.70, 0.71, 0.86, and 0.81, respectively (Nguyen et al., 2011). The drag coefficients of the air-water, air-ice and water-ice are set as 8.2×10^{-4}, 1.1×10^{-3} and 5.6×10^{-3}, respectively.

3. Evaluation results

To demonstrate the differences between observational datasets during evaluation of the temporal variability and linear trend in sea-ice extent, we compare the simulations against three observation datasets based on different algorithms; namely, the Bootstrap algorithm (obs1-Bootstrap), the NASA Team Algorithm (obs2-NASA Team) and the ASI algorithm (obs3-ASI).

The time series from 1991 to 2012 of the annual mean sea-ice extent in the Arctic from satellite observations and model simulations are compared in Fig. S1. Obvious uncertainties exist between the three observational datasets, and the sea-ice extents from obs3-ASI are generally lower than those from the obs1-Bootstrap and obs2-NASA Team. All of them, however, show similar annual variability in sea-ice extent. The trend in sea-ice extent from the simulations is

* The online version of this article can be found at https://doi.org/10.1007/s00376-020-9223-6.

-0.48×10^6 km^2 (10 yr)$^{-1}$, and the trends for the three observations are -0.68×10^6 km^2 (10 yr)$^{-1}$, -0.71×10^6 km^2 (10 yr)$^{-1}$ and -0.66×10^6 km^2 (10 yr)$^{-1}$, respectively. As presented in Vaughan et al. (2013), the trends in the sea-ice concentration, sea-ice extent and ice area, as inferred from data derived from the different algorithms, are generally compatible. Figure S2 shows the seasonality in the Arctic sea-ice extent over the period 1991–2012. The obvious disagreements between the monthly sea-ice extent of the obs3-ASI and the other two observations are prominent from January to June.

Figures S3 and S4 are results of individual RMSD analysis for observations from the NASA Team algorithm and the ASI algorithm. The results of the obs3-ASI are obviously different from the results of the obs1-Bootstrap and obs2-NASA Team. However, they all show that the magnitude of the "variance" in each year is substantially larger than that of the "bias", which suggests that the change in the "variance" is the dominant source contributing to the RMSD.

Figure S5 shows the variations of sea-ice extent in March and September for the period 1991–2012. Obs3-ASI retrieves much lower March sea-ice extents, which result in the differences among the three observations shown in Figs. S1 and S2. However, there is good agreement in the variability of March and September sea-ice extent between the three observations. Also, the simulations are better correlated with observations in the September for all three products. Furthermore, distributions of the linear trend in sea-ice concentration in March and September are shown in Fig. S6. The trends in sea-ice con-

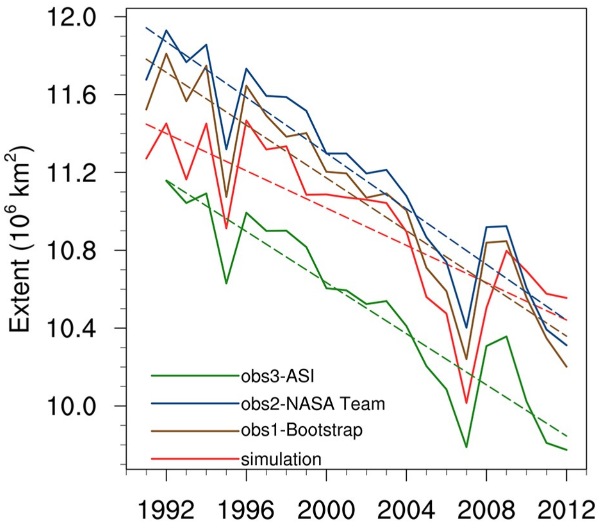

Fig. S1. Time series of the annual mean of monthly mean Arctic seaice extent from model simulations and three observations over the period 1991–2012.

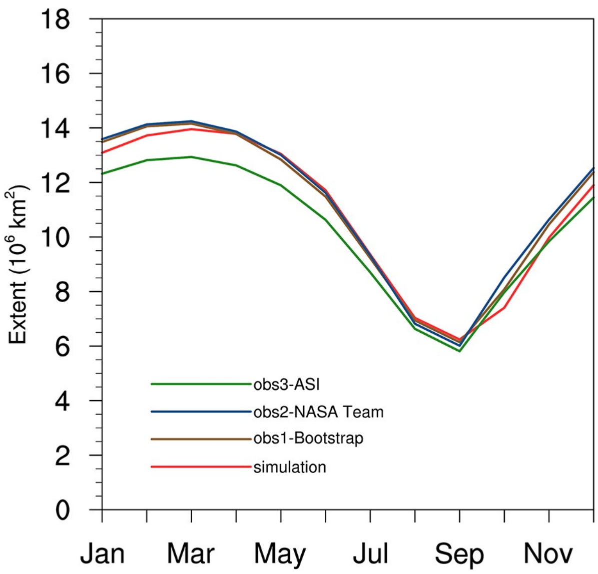

Fig. S2. Time series of the seasonal mean of monthly mean Arctic sea-ice extent from model simulations and three observations over the period 1991–2012.

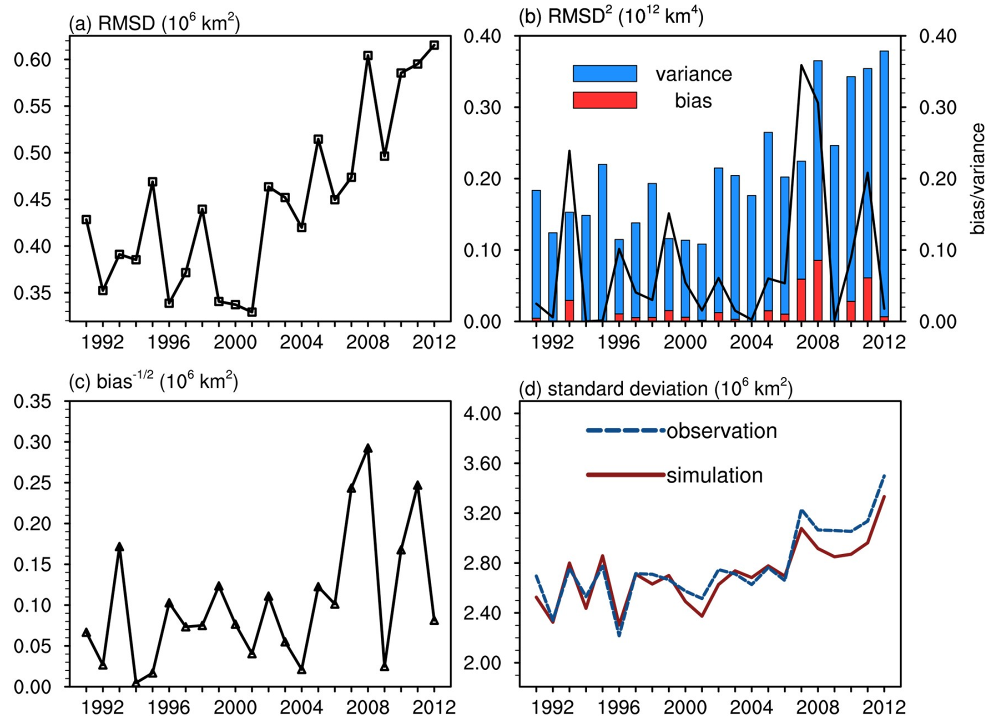

Fig. S3. Time series of the RMSD (10^6 km^2) between the detrended monthly sea-ice extent anomalies from simulations and those from observations based on the NASA Team algorithm and the RMSD-related terms over the period 1991–2012: (a) RMSD; (b) squared RMSD (histogram), consisting of "bias" and "variance", and the ratio of "bias" to "variance" (line); (c) absolute mean difference between simulations and observations; (d) standard deviation of simulations (red solid line) and observations (blue dashed line).

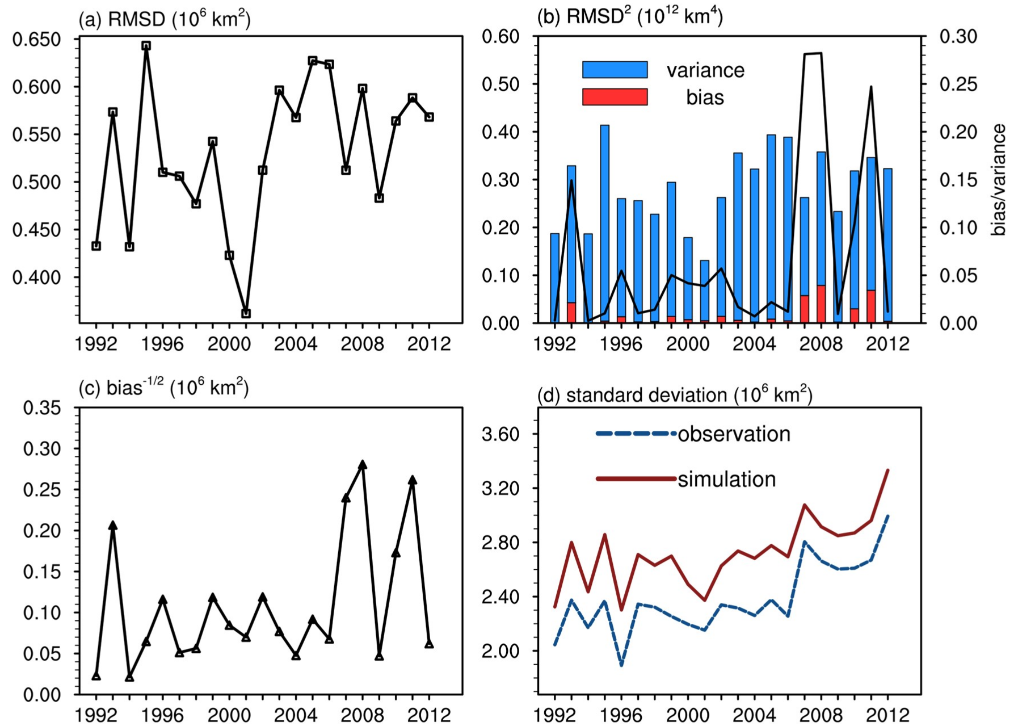

Fig. S4. Time series of the RMSD (10^6 km^2) between the detrended monthly sea-ice extent anomalies from simulations and those from observations based on the ASI algorithm and the RMSD-related terms over the period 1991–2012: (a) RMSD; (b) squared RMSD (histogram), consisting of "bias" and "variance", and the ratio of "bias" to "variance" (line); (c) absolute mean difference between simulations and observations; (d) standard deviation of simulations (red solid line) and observations (blue dashed line).

centration from different observations are similar.

Therefore, different algorithms could induce differences in the value of the sea-ice extent, but the variability and trends

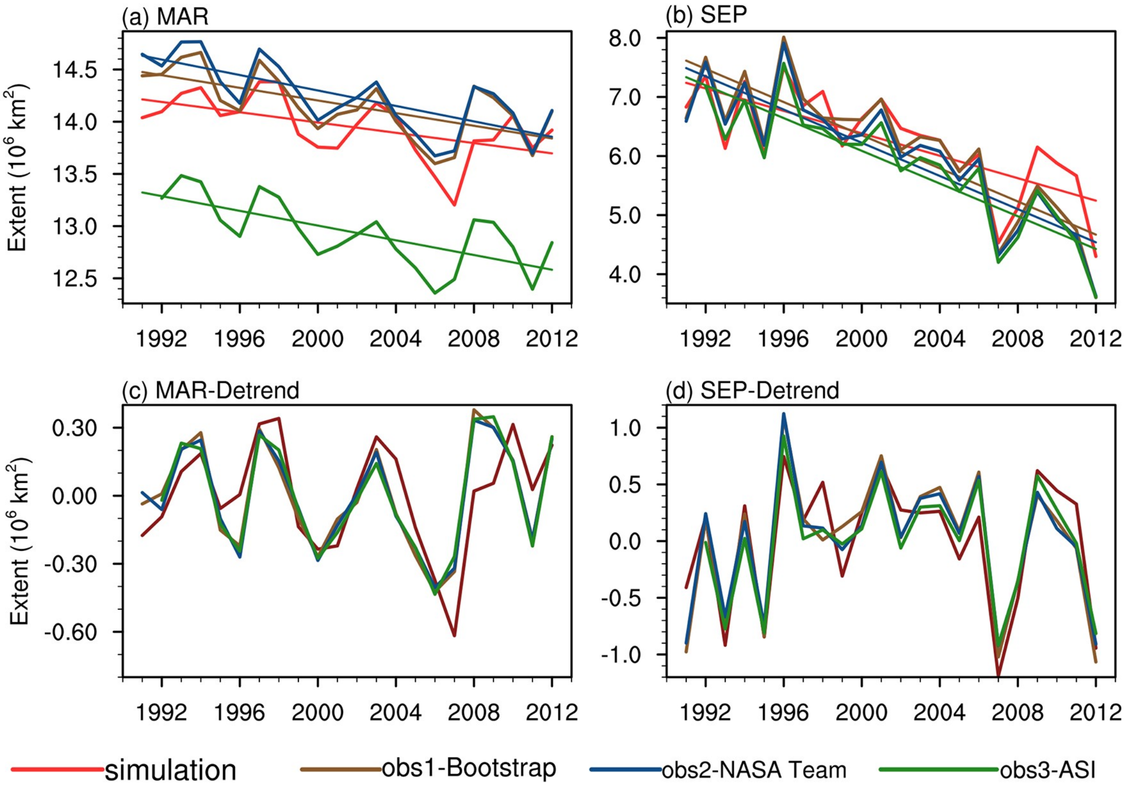

Fig. S5. Time series of monthly mean sea-ice extent in (a) March and (b) September over the period 1991–2012 and time series of detrended monthly sea-ice extent anomalies in (c) March and (d) September. Simulations are shown by the red line, and three observations from different algorithms are shown by the brown, blue and green line, respectively.

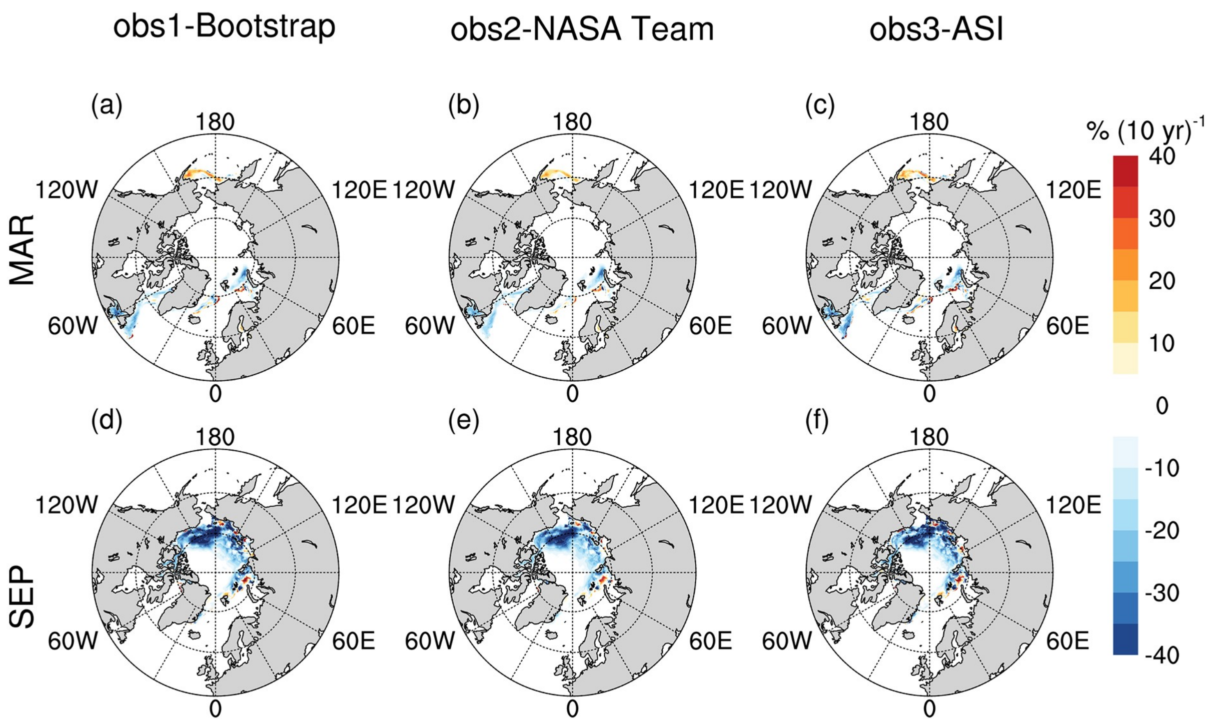

Fig. S6. Spatial distributions of the linear trends of sea-ice concentration in March over the period 1991–2012 from (a) obs1-Bootstrap, (b) obs2-NASA Team and (c) obs3-ASI. (d–f) As in (a–c), respectively, but for September.

in the sea-ice extent and sea-ice concentration from different observational datasets are consistent.

REFERENCES

Adcroft, A., J.-M. Campin, C. Hill, and J. Marshall, 2004: Implementation of an atmosphere ocean general circulation model on the expanded spherical cube. *Mon. Wea. Rev.*, **132**, 2845–2863, https://doi.org/10.1175/MWR2823.1.

Hibler III, W. D., 1979: A dynamic thermodynamic Sea Ice model. *J. Phys. Oceanogr.*, **9**, 815–846, https://doi.org/10.1175/1520-0485(1979)009<0815:ADTSIM>2.0.CO;2.

Losch, M., D. Menemenlis, J. M. Campin, P. Heimbach, and C. Hill, 2010: On the formulation of sea-ice models. Part 1: Effects of different solver implementations and parameterizations. *Ocean Modelling*, **33**, 129–144, https://doi.org/10.1016/j.ocemod.2009.12.008.

Marshall, J., C. Hill, L. Perelman, and A. Adcroft, 1997a: Hydrostatic, quasi - hydrostatic, and nonhydrostatic ocean modeling. *J. Geophys. Res.*, **102**, 5733–5752, https://doi.org/10.1029/96JC02776.

Marshall, J., A. Adcroft, C. Hill, L. Perelman, and C. Heisey, 1997b: A finite-volume, incompressible Navier Stokes model for studies of the ocean on parallel computers. *J. Geophys. Res.*, **102**, 5753–5766, https://doi.org/10.1029/96JC02775.

Nguyen, A. T., D. Menemenlis, and R. Kwok, 2011: Arctic ice-ocean simulation with optimized model parameters: Approach and assessment. *J. Geophys. Res.*, **116**, C04025, https://doi.org/10.1029/2010JC006573.

Semtner, A. J., Jr, 1975: A model for the thermodynamic growth of sea ice in numerical investigations of climate. *J. Phys. Oceanogr.*, **6**, 379–389, https://doi.org/10.1175/1520-0485(1976)006<0379:AMFTTG>2.0.CO;2.

Smith, W. H. F., and Sandwell D. T., 1997: Global sea floor topography from satellite altimetry and ship septh soundings. *Science*, **277**, 1956–1962, https://doi.org/10.1126/science.277.5334.1956.

Vaughan, D. G., and Coauthors, 2013: Observations: Cryosphere. *Climate Change 2013*: *The Physical Science Basis. Contribution of Working Group I to the Fifth Assessment Report of the Intergovernmental Panel on Climate Change*, T. F. Stocker et al., Eds., Cambridge University Press, 317–382.

Zhang, J. L., and W. D. Hibler III, 1997: On an efficient numerical method for modeling sea ice dynamics. *J. Geophys. Res.*, **102**, 8691–8702, https://doi.org/10.1029/96JC03744.